Intercomparison of Techniques to Correct for Attenuation of C-Band Weather Radar Signals

EUGENIO GORGUCCI AND GIANFRANCO SCARCHILLI

Istituto di Fisica dell'Atmosfera, CNR, Rome, Italy

V. CHANDRASEKAR

Colorado State University, Fort Collins, Colorado

P. F. MEISCHNER AND M. HAGEN

DLR, Institut für Physik der Atmosphäre, Oberpfaffenhofen, Germany

(Manuscript received 23 May 1997, in final form 30 December 1997)

ABSTRACT

Quantitative application of radar measurements at C band requires correction for attenuation. Algorithms to correct for attenuation and differential attenuation are evaluated based on theoretical analysis as well as radar data. The error structure of three different attenuation correction algorithms based on (a) reflectivity, (b) reflectivity and differential reflectivity, and (c) specific differential propagation phase is analyzed. The error structure of two algorithms to correct the differential attenuation based on (a) reflectivity and differential reflectivity, and (b) specific differential propagation phase is presented. Data from the polarimetric C-band Doppler radar POLDIRAD operated by DLR (Germany) are utilized to intercompare the attenuation and differential attenuation correction algorithms. Radar data and theoretical analysis show that the attenuation correction algorithm using reflectivity and differential reflectivity agrees well with the attenuation correction algorithm based on specific differential phase. Similarly, radar data and theoretical analysis indicate that the algorithms to correct for differential attenuation compare well with each other. In addition the fractional standard error of comparison between the algorithms to correct for attenuation and differential attenuation is in good agreement with theoretical results, providing an indirect verification of the accuracies of the algorithms.

1. Introduction

C-band radar systems are widely used in Europe for meteorological applications. S-band weather radar systems are commonly used in the United States for operational applications requiring long-range coverage such as few hundred kilometers. Radars that operate at higher frequencies offer the advantage of lower cost resulting from smaller antenna size compared to lower-frequency radars having the same spatial resolution. However, the resulting spatial resolution at lower cost is offset by attenuation problems. Quantitative interpretation of echo powers at C-band frequencies requires correction for attenuation to avoid errors in estimating precipitation. Attenuation correction for C-band radars can be done with different methods depending on the type of measurements involved. Conventional attenuation correction procedures involve a Z–α relation where the specific attenuation (α) is related to the reflectivity factor (Z) by a power law. However, the absence of a unique relation made them difficult to use (Aydin et al. 1989). Aydin et al. (1989) introduced an attenuation correction procedure for dual-polarization radars parameterizing the ratio of specific attenuation and reflectivity factor (α/Z) in terms of the differential reflectivity (Z_{DR}). Bringi et al. (1990) examined an attenuation correction procedure based on the relationship between the specific differential phase (K_{DP}) and specific attenuation.

Excessively attenuated radar echoes can be spotted on reflectivity maps such as range streaks. However, when attenuation is not excessive (such as a few decibels), the effects are difficult to observe. C-band radar signals fall under this category, where the typical attenuation levels encountered are neither excessive (several tens of decibels) nor negligible (less than 0.15 dB). This poses a problem for applications involving quantitative measurement of reflectivity. Scarchilli et al. (1993) have shown from theoretical studies that when the total attenuation is small (~1 dB) the attenuation correction process introduces errors, which outweigh the

Corresponding author address: Dr. Eugenio Gorgucci, Istituto di Fisica dell'Atmosfera, Via del Fosso del Cavaliere, 00133 Rome, Italy.
E-mail: gorgucci@radar.ifa.rm.cnr.it

© 1998 American Meteorological Society

benefit of the attenuation correction. Gorgucci et al. (1995) introduced a simplified version of the attenuation correction procedure suggested by Aydin et al. (1989) by directly parameterizing the specific and differential attenuation in terms of radar measurements such as Z and $Z_{\rm DR}$.

In this paper we conduct a detailed study intercomparing the various attenuation correction procedures using theoretical simulations as well as data collected by the C-band polarization diversity radar POLDIRAD operated by Deutsche Forschungsanstalt für Luft- und Raumfahrt (DLR) (Germany). The data reported in this paper were collected as part of a collaborative program between the Radar Meteorology Group of the Institute of Atmospheric Physics (IFA) of the National Research Council (CNR) of Italy and the DLR Institute of Atmospheric Physics of Germany.

Our paper is organized as follows: Section 2 presents the various attenuation correction procedures. In section 3 we conduct an error study of the attenuation correction procedures considered. Section 4 describes the dataset and instrumentation. In section 5 the intercomparison of the attenuation correction estimates from radar data is presented. Section 6 summarizes the important results of this paper.

2. Attenuation correction procedures at C band

Reflectivity measurements at C band are affected by attenuation of radar signals passing through precipitation that exists between the radar and the measurement cell. Differential reflectivity measurements at C band are similarly affected by the differential attenuation between horizontally (H) and vertically (V) polarized waves. The distributions of raindrop size and shape determine the values of the radar observables as, for example, the reflectivity factor Z, the differential reflectivity $Z_{\rm DR}$, and the specific attenuation α. The gamma distribution model adequately describes the natural variation of the raindrop size distribution (RSD). This is given by

$$N(D) = N_0 D^{\mu} \exp\left[\frac{-(3.67 + \mu)D}{D_0}\right], \qquad (1)$$

where N_0, D_0, and μ are the parameters of the RSD and D_0 is the median volume diameter (Ulbrich 1983). The equilibrium shape of a raindrop falling at its terminal fall speed is determined by the balance between the forces due to surface tension, hydrostatic pressure, and aerodynamic pressure from airflow around the drop. The shape of a raindrop can be approximated by an oblate spheroid with the axis ratio (b/a) of the drop approximated by the relationship

$$\frac{b}{a} = 1.03 - 0.062 D_e, \qquad (2)$$

where D_e is the equivolumetric spherical diameter of a raindrop in millimeters, and a and b are the major and minor axes of the drop, respectively (Beard and Chuang 1987; Chandrasekar et al. 1988). The radar measurements such as the reflectivity factor at horizontal and vertical polarization $Z_{H,V}$ and $Z_{\rm DR}$ can be expressed in terms of the RSD as follows:

$$Z_{H,V} = \frac{\lambda^4}{\pi^5 |K|^2} \int \sigma_{H,V}(D) N(D)\, dD, \qquad (3)$$

where $\sigma_{H,V}$ are the radar cross sections of raindrops corresponding to H and V polarizations,

$$Z_{\rm DR} = 10 \log\left(\frac{Z_H}{Z_V}\right) \qquad (4)$$

(Seliga and Bringi 1976). We refer to the article by Bringi and Hendry (1990) for details regarding polarization diversity measurements.

The specific attenuation at horizontal polarization, α_H (attenuation per unit length), and the specific differential attenuation, α_D (differential attenuation per unit length), between the two polarization states H and V are related to the RSD as follows (Bringi et al. 1990):

$$\alpha_{H,V} = 4.343 \times 10^{-3}\, \mathcal{J}m \int f_{H,V} N(D)\, dD \qquad (5)$$

and

$$\alpha_D = \alpha_H - \alpha_V, \qquad (6)$$

where $f_{H,V}$ are the forward scattering amplitudes at H and V polarization states, respectively, and $\mathcal{J}m$ refers to imaginary part of a complex number. Scarchilli et al. (1993) have studied the variability of α_H and α_D as a function of rainfall rate at C-band frequencies. Their results show that specific attenuation rates can be as high as 0.5 dB km^{-1} and α_D can be as high as 0.15 dB km^{-1}. These results show that the absolute attenuation through large rain cells could be easily several decibels in magnitude, while comparable values of differential attenuation could also reach as much as a few decibels.

There are essentially three different ways to correct for the attenuation caused by precipitation. The first is based on the conventional procedure, which involves estimation of attenuation using a power-law relation to approximate α_H in term of Z_H (Hildebrand 1978). The second procedure utilizes polarimetric measurements and was introduced by Aydin et al. (1989) to correct for the attenuation in C band parameterizing the relationship between the ratio (α_H/Z_H) and $Z_{\rm DR}$. Gorgucci et al. (1995) simplified this procedure to directly estimate α_H and α_D using Z_H and $Z_{\rm DR}$. Bringi et al. (1990) and Scarchilli et al. (1993) examined a third procedure to correct for attenuation and differential attenuation using $K_{\rm DP}$ measurements. In this paper we conduct a detailed study of the error structure of all these procedures and also present an intercomparison between the different techniques.

TABLE 1. The variation of the coefficients in $\hat{\alpha}_H$ with temperature.

T (°C)	C_H	a_1	b_1
0.5	9.89×10^{-6}	0.95	−0.130
2.0	9.03×10^{-6}	0.96	−0.124
5.0	7.78×10^{-6}	0.97	−0.119
10.0	6.31×10^{-6}	0.97	−0.104
20.0	4.02×10^{-6}	0.98	−0.080

TABLE 2. The variation of the coefficients in $\hat{\alpha}_D$ with temperature.

T (°C)	C_D	a_2	b_2
0.5	6.47×10^{-7}	1.02	−0.052
2.0	6.84×10^{-7}	1.02	−0.050
5.0	6.62×10^{-7}	1.01	−0.044
10.0	5.86×10^{-7}	1.02	−0.030
20.0	5.03×10^{-7}	1.01	−0.011

The specific attenuation α_H and differential attenuation α_D can be parameterized in terms of Z_H and $Z_{\rm DR}$ as

$$\hat{\alpha}_H = C_H Z_H^{\alpha_1} 10^{b_1 Z_{\rm DR}} \tag{7}$$

$$\hat{\alpha}_D = C_D Z_H^{\alpha_2} 10^{b_2 Z_{\rm DR}}. \tag{8}$$

The coefficients C_H, C_D, a_1, a_2, b_1, and b_2 vary with temperature, but not extensively. Tables 1 and 2 show the coefficients in the parameterizations (7) and (8) as a function of temperature. The parameterization for 10°C is used in this paper (to fit the environment of the radar data presented). Figure 1a shows a scatterplot of $\hat{\alpha}_H$ versus α_H, whereas Fig. 1b shows $\hat{\alpha}_D$ versus α_D for different RSDs (Ulbrich 1983). Figures 1a and 1b show the ability of the parameterization in (7) and (8) to estimate the specific attenuation and differential attenuation. The estimates $\hat{\alpha}_H$ and $\hat{\alpha}_D$ follow the actual attenuation values fairly well, with a very narrow scatter and the correlation coefficients are 0.998 and 0.991, respectively. For completion we have also parameterized α_H in terms of the reflectivity factor Z_H only as

$$\hat{\alpha}_Z = C_Z Z_H^{\alpha_3}. \tag{9}$$

Figure 2 shows a scatterplot of $\hat{\alpha}_Z$ versus α_H, and Table 3 shows the variability of the coefficients in (9), which are obtained with the same technique as in (7) and (8), as a function of temperature. We can see from a comparison of Fig. 1a with Fig. 2 that the algorithm given by (7) tracks attenuation significantly better than the algorithm given by (9) using reflectivity only.

Attenuation and differential attenuation cumulatively increase with the range. Therefore, echoes from cells close to the radar are not attenuated as much as the echoes from storm cells farther from the radar. It can be assumed that the closest echo is not attenuated and the attenuation cumulatively adds up from that point. Therefore, the attenuation is estimated from the first range echo point and then the reflectivities are corrected sequentially in range. A cumulative procedure in range is used similar to the one used by Aydin et al. (1989) to correct for attenuation and differential attenuation. The algorithm for attenuation is as follows:

$$(\hat{Z}_H)_n = (Z_H^m)_n + \sum_{i=1}^{n-1} (\hat{\alpha}_H)_i \, \Delta r, \tag{10}$$

where $(\hat{Z}_H)_n$ is the reflectivity at range bin n corrected for attenuation, $(Z_H^m)_n$ is the measured reflectivity at range bin n, Δr is the range gate spacing, and $(\hat{\alpha}_H)_i$ is the estimate (7) of the specific attenuation at range bin

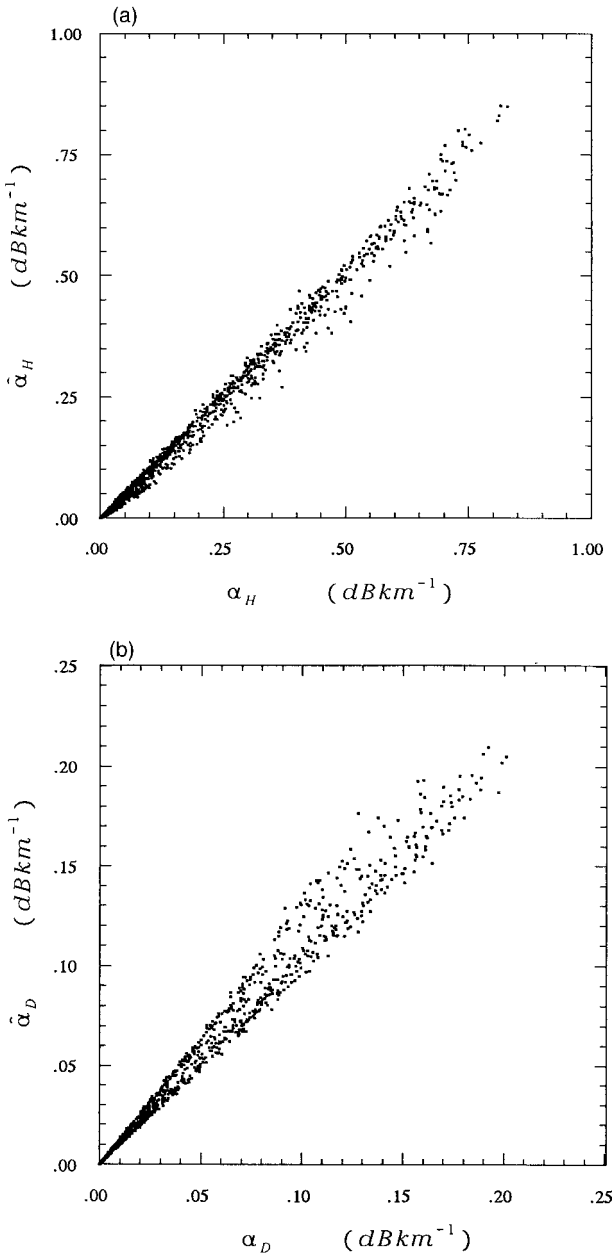

FIG. 1. (a) Scatterplot of the estimate of specific attenuation ($\hat{\alpha}_H$) using Z_H and $Z_{\rm DR}$ as a function of specific attenuation (α_H) for different RSDs. (b) Scatterplot of the estimate of specific differential attenuation ($\hat{\alpha}_D$) using Z_H and $Z_{\rm DR}$ as a function of specific differential attenuation (α_D) for different RSDs.

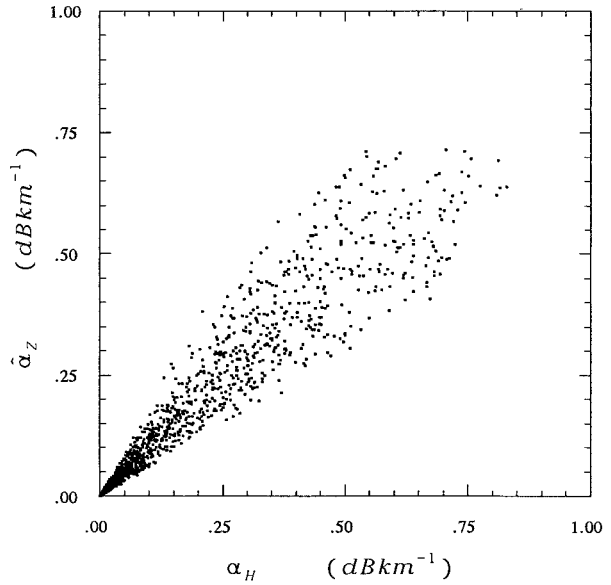

FIG. 2. Scatterplot of the estimate of specific attenuation ($\hat{\alpha}_Z$) using Z_H as a function of specific attenuation (α_H) for different RSDs.

i. It should be noted here that reflectivity estimate at range $(\hat{Z}_H)_i$ is corrected for attenuation up to $(i - 1)$ range bins. Similarly the differential reflectivity measurements can be corrected as

$$(\hat{Z}_{\mathrm{DR}})_n = (Z^m_{\mathrm{DR}})_n + \sum_{i=1}^{n-1} (\hat{\alpha}_D)_i \, \Delta r, \tag{11}$$

where $(\hat{Z}_{\mathrm{DR}})_n$ is the estimate of differential reflectivity at range bin n corrected for differential attenuation, $(Z^m_{\mathrm{DR}})_n$ is the measured differential reflectivity at range bin n, and $(\hat{\alpha}_D)_i$ is the estimate (8) of the specific differential attenuation at range i. Similar to the parameterization in terms of Z_H and Z_{DR}, α_H and α_D can also be parameterized in terms of K_{DP} as follows:

$$\hat{\alpha}^*_H = C^*_H K_{\mathrm{DP}} \tag{12}$$

and

$$\hat{\alpha}^*_D = C^*_D K_{\mathrm{DP}}. \tag{13}$$

Table 4 shows the coefficients in the parameterizations (12) and (13) at C band as a function of temperature. Figure 3a shows a scatterplot of $\hat{\alpha}^*_H$ versus the true value of α_H, whereas Fig. 3b shows $\hat{\alpha}^*_D$ versus the true value of α_D for different RSDs.

The range-cumulative two-way differential phase

TABLE 3. The variation of the coefficients in $\hat{\alpha}_Z$ with temperature.

T (°C)	C_Z	a_3
0.5	7.16×10^{-5}	0.73
2.0	4.36×10^{-5}	0.77
5.0	4.70×10^{-5}	0.76
10.0	2.16×10^{-5}	0.82
20.0	1.69×10^{-5}	0.83

TABLE 4. The variation of the coefficients in $\hat{\alpha}^*_H$ and $\hat{\alpha}^*_D$ with temperature.

T (°C)	C^*_H	C^*_D
0.5	7.17×10^{-2}	1.44×10^{-2}
2.0	6.98×10^{-2}	1.40×10^{-2}
5.0	6.53×10^{-2}	1.30×10^{-2}
10.0	5.88×10^{-2}	1.23×10^{-2}
20.0	4.85×10^{-2}	1.10×10^{-2}

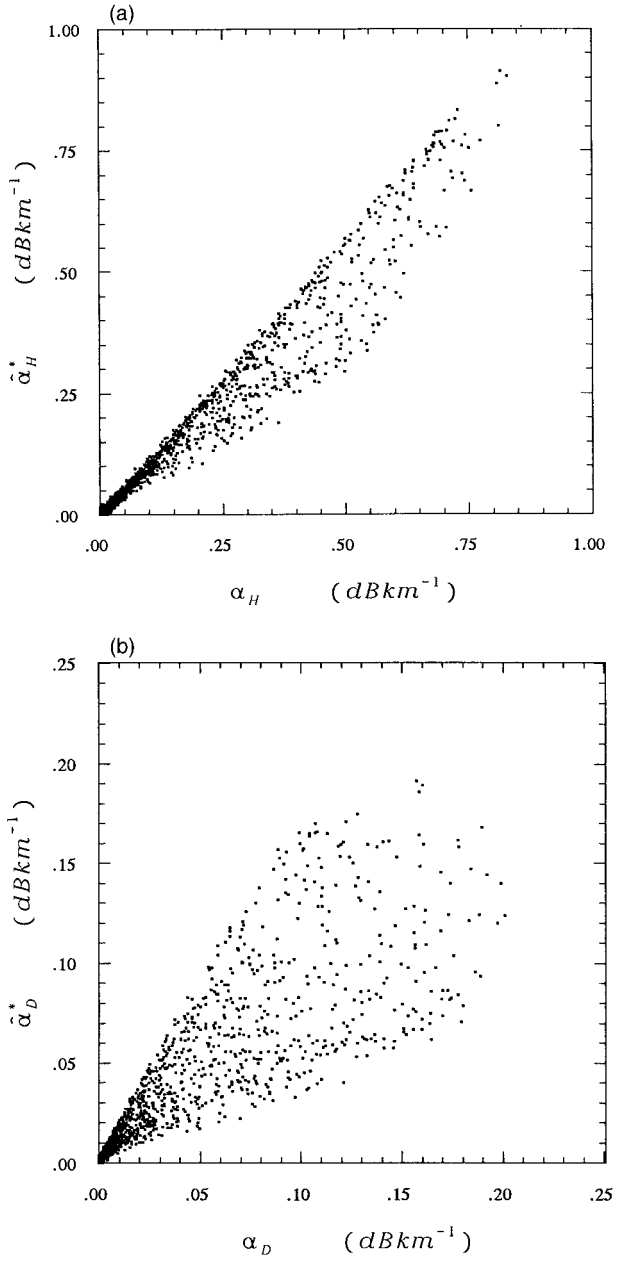

FIG. 3. (a) Scatterplot of the estimate of specific attenuation ($\hat{\alpha}^*_H$) using K_{DP} as a function of specific attenuation ($\hat{\alpha}_H$) for different RSDs. (b) Scatterplot of the estimate of specific differential attenuation ($\hat{\alpha}^*_D$) using K_{DP} as a function of specific differential attenuation (α_D) for different RSDs.

TABLE 5. Fractional standard error in the estimation of the different algorithms due to the parameterization (first column) and including measurement errors averaged over a 12-km path (second column).

Algorithm	FSE (%)	FSE (%)
$\hat{\alpha}_H$	11.9	10.9
$\hat{\alpha}_D$	24.1	19.1
$\hat{\alpha}_Z$	38.4	34.3
$\hat{\alpha}_H^*$	27.5	26.9
$\hat{\alpha}_D^*$	77.8	65.2

shift (Φ_{DP}), attenuation (A_H), and differential attenuation (A_D) can be expressed as

$$\Phi_{DP} = 2\int_0^{R_c} K_{DP}(r)\,dr, \tag{14}$$

$$A_H = 2\int_0^{R_c} \alpha_H(r)\,dr, \tag{15}$$

and

$$A_D = 2\int_0^{R_c} \alpha_D(r)\,dr, \tag{16}$$

where R_c is the range to the observation cell. Since α_H and α_D are nearly related to K_{DP} in rainfall, we can estimate A_H and A_D directly from Φ_{DP} measurements, which can be used to correct attenuation and differential attenuation. In the following section we study the error structure of the above-mentioned attenuation correction procedures.

3. Error structure of attenuation correction procedures

There are potentially two sources of errors that can affect these correction algorithms, namely, (a) random measurement fluctuations and (b) error in the absolute gain of the radar system (which results as a bias in the estimate of Z_H). The effect of random measurement fluctuations is analyzed in this paper using radar signal simulations. Algorithms (7), (9), and (12) as well as (8) and (13) can be used to estimate α_H and α_D, respectively. Table 5 summarizes the accuracies in the estimation of specific and differential attenuation using the various techniques discussed in this paper. The accuracy is described by the fractional standard error (FSE), which is defined as the standard error normalized with respect to the mean. The first column in Table 5 shows the accuracy in the algorithms due to the parameterization process. We can see in Table 5 that $\hat{\alpha}_H$, $\hat{\alpha}_H^*$, and $\hat{\alpha}_Z$ can estimate α_H to an accuracy of 11.9%, 27.5%, and 38.4%, respectively. The above error estimates were obtained by averaging over many different RSDs (Ulbrich 1983). Similarly $\hat{\alpha}_D$ and $\hat{\alpha}_D^*$ can estimate α_D to an accuracy of 24.1% and 77.8%, respectively. We need to note here that the above accuracies are reported in the absence of measurement error. However, measurement errors play a significant role in the error structure of all algorithms. We have used radar system simulations (Chandrasekar et al. 1986) to study the effect of measurement errors on the attenuation correction algorithms. The principal assumptions in our simulation are as follows: Gaussian Doppler spectrum with spectrum width of 2 m s^{-1}, pulse repetition time of 1 ms, sample pairs number of 64, wavelength of 5.5 cm, and cross correlation between the horizontal and vertical polarized return signals $\rho_{H,V}$ of 0.99. We note here that Z_H and Z_{DP} are point measurements (measured at each range gate), whereas K_{DP} is estimated as the slope of the Φ_{DP} range profile. For estimating K_{DP} we have assumed a uniform path. We have considered two pathlengths, namely, 6 and 12 km, corresponding to 20 and 40 gates with a gate spacing of 300 m. The second column in Table 5 shows the error in the algorithms in the presence of measurement errors after averaging over a 12-km path. We can see that $\hat{\alpha}_H$ and $\hat{\alpha}_D$ can estimate α_H and α_D to an accuracy of 11% and 19%, respectively. Similarly, $\hat{\alpha}_H^*$ and $\hat{\alpha}_D^*$ with K_{DP} estimated averaging over a 12-km path can estimate α_H and α_D to an accuracy of 27% and 65%, respectively. In addition, $\hat{\alpha}_Z$ can estimate α_H to an accuracy of 35%. Since a 12-km path may be considered too long for uniform precipitation approximation, we have repeated the computations for a 6-km path and the results were similar. Note here that even though we have used 6- and 12-km paths to estimate an average specific attenuation for analysis purpose, it does not mean that the attenuation correction is affected. The cumulative attenuation due to the rain cell along a path is represented by an average value over the path. This is done strictly to reduce statistical errors in comparisons, and the attenuation correction procedure can be applied to any pathlength. Table 5 provides an idea about the average accuracy of the attenuation correction procedure. However, the accuracy also changes with the value of specific attenuation. Figure 4 shows the FSE in the estimates $\hat{\alpha}_H$, $\hat{\alpha}_H^*$, and $\hat{\alpha}_Z$ as a function of α_H. The FSEs are obtained for a 12-km path, including the effect of measurement errors. We can see in Fig. 4 that the specific attenuation can be estimated to an accuracy between 5% and 25% when $\alpha_H > 0.2$ dB km^{-1}. Among the algorithms to estimate specific attenuation, $\hat{\alpha}_H$ has the lowest error. However, the estimate $\hat{\alpha}_H^*$ has an important advantage that it is not at all affected by errors in radar calibration. Large absolute calibration errors can affect the $\hat{\alpha}_H$ estimates significantly, as discussed by Aydin et al. (1989). Therefore, it is important to ensure that the radar is well calibrated before applying reflectivity-based attenuation correction algorithms. Another point to note in Fig. 4 is that, when specific attenuation is negligible (<0.05 dB km^{-1}, light rain), the accuracy of $\hat{\alpha}_Z$ and $\hat{\alpha}_H$ estimates is comparable. Figure 5 shows the FSE of $\hat{\alpha}_D$ and $\hat{\alpha}_D^*$ as a function of α_D, respectively. The result of Fig. 5 was obtained assuming a pathlength of 12 km, including the effect due tob measurement errors. For correcting differential attenuation we can see that

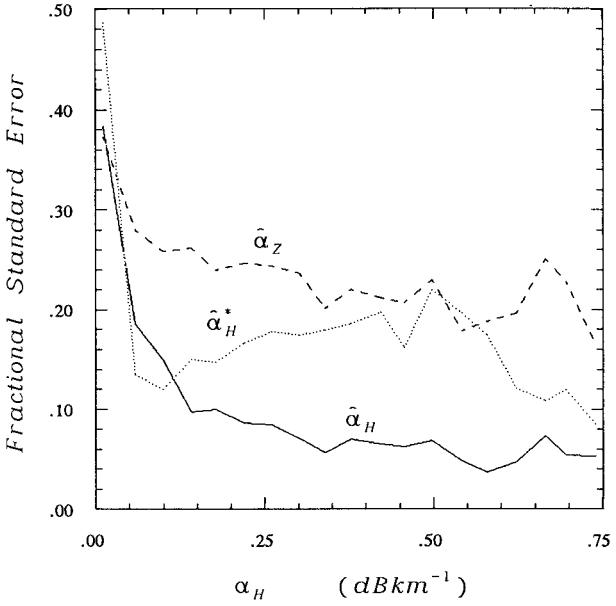

FIG. 4. Fractional standard error of $\hat{\alpha}_H$, $\hat{\alpha}^*_H$, and $\hat{\alpha}_Z$ given as a function of specific attenuation α_H. The estimates were obtained over a 12-km path.

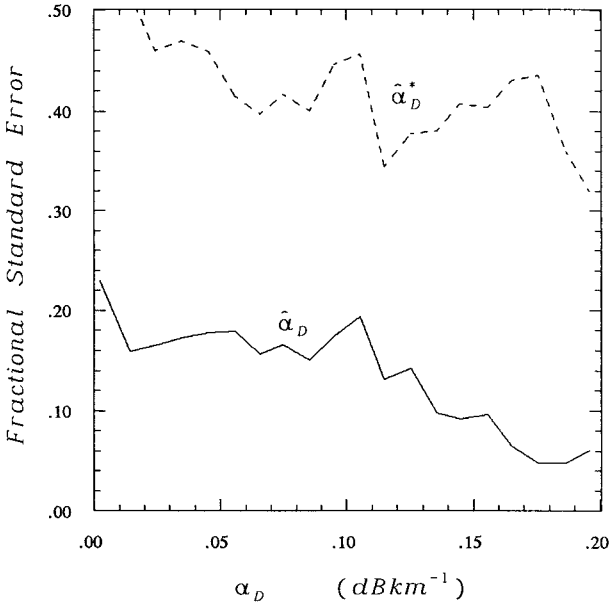

FIG. 5. Fractional standard error of $\hat{\alpha}_D$ and $\hat{\alpha}^*_D$ given as a function of specific diffberential attenuation α_D. The estimates were obtained over a 12-km path.

$\hat{\alpha}_D$ is significantly more accurate than $\hat{\alpha}^*_D$. It can be seen in Fig. 5 that α_D can be estimated to an accuracy of 10%–15% using algorithm $\hat{\alpha}_D$ and 40% using algorithm $\hat{\alpha}^*_D$ when $\alpha_D > 0.05$ dB km^{-1}. Once again we need to note that $\hat{\alpha}^*_D$ is immune to absolute calibration errors.

4. Radar data description

The radar data used in this paper were collected by the polarimetric C-band Doppler radar POLDIRAD operated by DLR. Details on POLDIRAD can be found in Schroth et al. (1988). The data were collected as part of the collaborative program between IFA of CNR of Italy and the DLR Institute of Atmospheric Physics of Germany. The dataset analyzed here was collected on 29 August 1995 during the passage of a cold front from the north, providing an excellent opportunity to observe the storm over an extended period of time. This cold front stalled over the Alps, leading to long-lasting precipitation on the northern Alpine foreland. The radar data were collected in a plan position indicator (PPI) mode, and the multiparameter radar variables Z_H, Z_{DR}, and Φ_{DP} were measured by averaging 64 sample pairs at a pulse repetition frequency of 1200. The data used in this paper were collected at 1° elevation, and the data analyzed were confined to ranges less than 50 km. This ensured that there was no contamination by the melting layer. The attenuation correction procedures described in section 2 were applied to the radar data and $\hat{\alpha}_H$, $\hat{\alpha}^*_H$, $\hat{\alpha}_Z$, $\hat{\alpha}_D$, and $\hat{\alpha}^*_D$ were estimated.

5. Experimental results

For comparative analysis the radar data of each measured ray were divided into intervals of 12-km pathlength. In each 12-km segment K_{DP} was estimated using a straight line fit to the Φ_{DP} profile. Subsequently, average values of $\hat{\alpha}_H$, $\hat{\alpha}^*_H$, and $\hat{\alpha}_Z$ as well as $\hat{\alpha}_D$and $\hat{\alpha}^*_D$ were computed. Figure 6a shows a comparison of $\hat{\alpha}_H$ versus $\hat{\alpha}^*_H$. The vertical bars indicate the standard deviation about the mean value. We can see in Fig. 6a that $\hat{\alpha}_H$ and $\hat{\alpha}^*_H$ agree fairly well with a slope of 0.95. The bias for the comparison between $\hat{\alpha}_H$ and $\hat{\alpha}^*_H$ was found to be 4% (very low). The results of Fig. 6a show that the two estimates agree very well. The maximum specific attenuation encountered on a 12-km path was 0.22 dB km^{-1}, which corresponds to a two-way cumulative attenuation of 5.3 dB, thereby indicating the importance of the attenuation correction. Figure 6b shows a comparison of $\hat{\alpha}_Z$ and $\hat{\alpha}^*_H$. The vertical bars again indicate standard deviation. We can see in Fig. 6b that there is a bias in $\hat{\alpha}_Z$. This is because the arbitrary α_Z–Z relation used in this paper is not the best α_Z–Z relation corresponding to the data. The α_Z–Z relation exhibits a wide variability very similar to Z–R relations. Figure 7 shows the FSE in the comparison of $\hat{\alpha}_H$ and $\hat{\alpha}_Z$ as a function of $\hat{\alpha}^*_H$. Also shown in Fig. 7 is the FSE between $\hat{\alpha}_H$ and $\hat{\alpha}^*_H$ that was computed based on simulation including the effect of measurement errors. We need to note here that the FSE of comparison between $\hat{\alpha}_H$ and $\hat{\alpha}^*_H$ includes error in the estimation of α_H and α^*_H. Similarly, the FSE of comparison between $\hat{\alpha}_Z$ and $\hat{\alpha}^*_H$ includes errors in the estimation of α_Z and α^*_H. In general a fairly good agreement exists between experimentally observed FSE be-

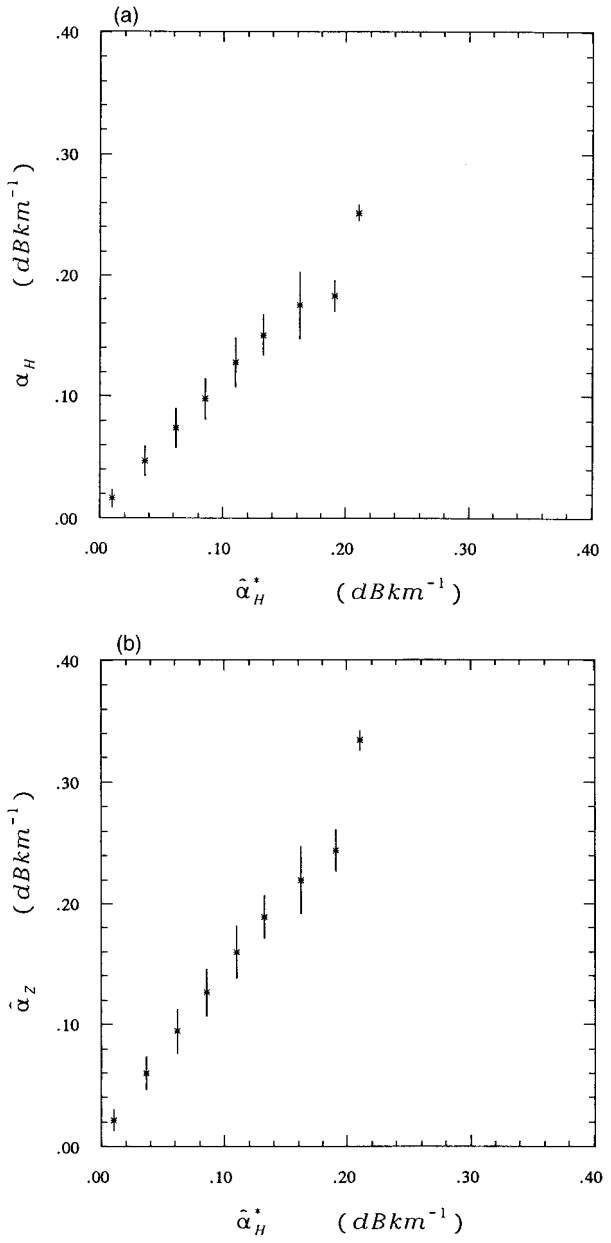

FIG. 6. (a) Comparison of the estimates $\hat{\alpha}_H$ and $\hat{\alpha}_H^*$ from the radar data collected by DLR radar. The dots indicate the mean and the vertical bars denote standard deviation. (b) Comparison of the estimates $\hat{\alpha}_Z$ and $\hat{\alpha}_H^*$ from the radar data collected by DLR radar. The dots indicate the mean and the vertical bars denote standard deviation.

tween $\hat{\alpha}_H$ and $\hat{\alpha}_H^*$ with simulation results. The agreement is not perfect, which can be due to many reasons—one of them can be the difference in the ambient temperature of the environment where data was obtained and the parameterization used. In addition it can be seen in Fig. 7 that the FSE of comparison between $\hat{\alpha}_Z$ and $\hat{\alpha}_H^*$ is higher than the FSE of comparison between $\hat{\alpha}_H$ and $\hat{\alpha}_H^*$. This is due to the biased nature of $\hat{\alpha}_Z$, which can be seen in Fig. 6b. Similarly, Fig. 8 shows the comparison of $\hat{\alpha}_D$ versus $\hat{\alpha}_D^*$. It can be seen in Fig. 8 that the two estimates are of the same order and agree reasonably well. The vertical bars indicate standard deviation in the comparison. Figure 9 shows the FSE in the comparison of $\hat{\alpha}_D$ and $\hat{\alpha}_D^*$. Also shown in Fig. 9 is the FSE between $\hat{\alpha}_D$ and $\hat{\alpha}_D^*$ that was computed based on simulation including the effect of measurement error.

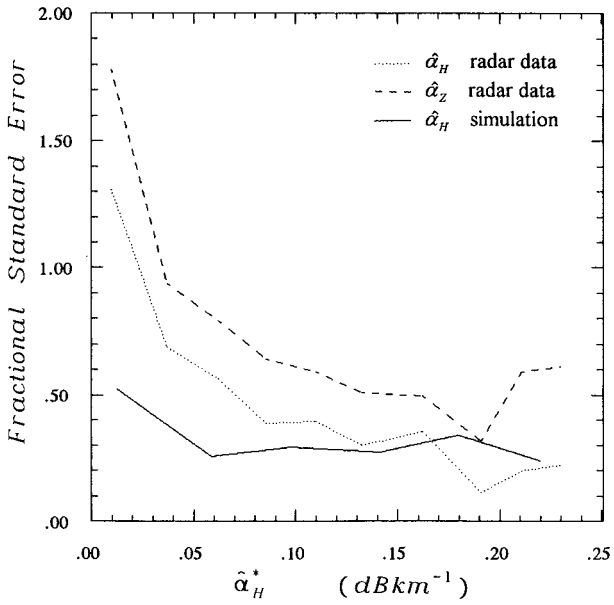

FIG. 7. Fractional standard error of the comparison between $\hat{\alpha}_H$ and $\hat{\alpha}_H^*$ (dotted line) as well as $\hat{\alpha}_Z$ and $\hat{\alpha}_H^*$ (dashed line) shown as a function of $\hat{\alpha}_H^*$ for the data collected by DLR radar. The solid line shows the FSE of the comparison between $\hat{\alpha}_H$ and $\hat{\alpha}_H^*$ as a function of $\hat{\alpha}_H^*$ obtained from simulation.

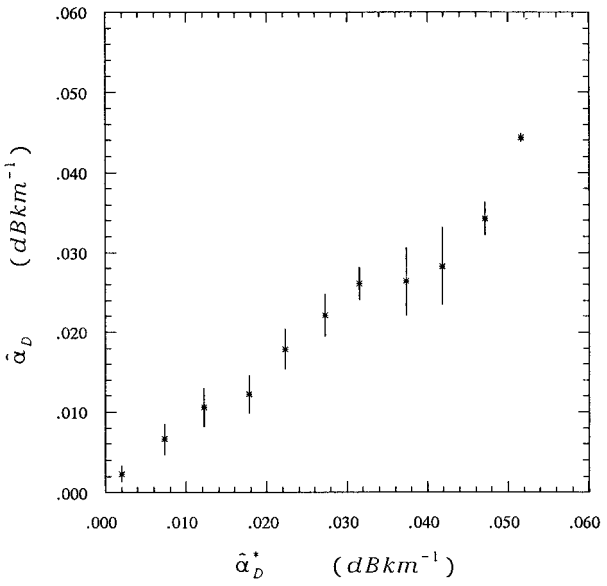

FIG. 8. Comparison of the estimates $\hat{\alpha}_D$ and $\hat{\alpha}_D^*$ from radar data collected by DLR radar. The dots indicate the mean and the vertical bars indicate the standard deviation.

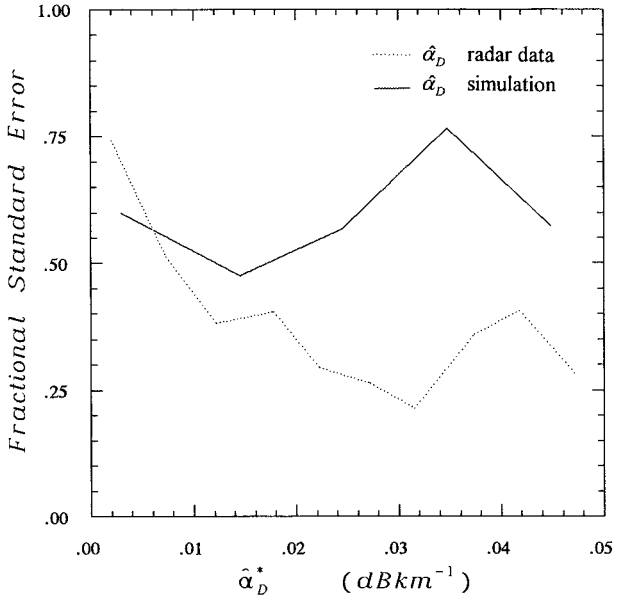

FIG. 9. Fractional standard error of the comparison between $\hat{\alpha}_D$ and $\hat{\alpha}_D^*$ (dotted line) shown as a function of $\hat{\alpha}_D^*$ for the data collected by DLR radar. The solid line shows the FSE of the comparison between $\hat{\alpha}_D$ and $\hat{\alpha}_D^*$ as a function of $\hat{\alpha}_D^*$ obtained from simulation.

Note here that the FSE of comparison between $\hat{\alpha}_D$ and $\hat{\alpha}_D^*$ includes errors in the estimation of α_D and α_D^*. The experimentally observed FSE between $\hat{\alpha}_D$ and $\hat{\alpha}_D^*$ is of the same order as that from simulation. The agreement is not as good as that between $\hat{\alpha}_H$ and $\hat{\alpha}_H^*$, primarily because $\hat{\alpha}_D$ and $\hat{\alpha}_D^*$ have more scatter in the parameterization process compared to estimates of α_H.

6. Summary and conclusions

Algorithms to correct for attenuation at C-band frequencies are analyzed. C-band radar measurements of reflectivity are affected by absolute attenuation and the measurements of differential reflectivity are affected by differential attenuation. Quantitative application of echo power requires correction for attenuation and differential attenuation. Two attenuation correction algorithms, namely, one using Z_H and $Z_{\rm DR}$ and the other using $K_{\rm DP}$, are studied based on theoretical analysis as well as data collected by a C-band dual-polarized radar. Theoretical analysis shows that the algorithm to correct for attenuation based on Z_H and $Z_{\rm DR}$ can correct attenuation to an accuracy of 10% when the specific attenuation is more than 0.2 dB km^{-1}. Similarly, the algorithm to correct attenuation based on $K_{\rm DP}$ can correct attenuation to an accuracy of 20%. Though the algorithm $\hat{\alpha}_H^*$ has only half the accuracy of $\hat{\alpha}_H$, it has the advantage that it is immune to radar calibration errors. A large error in radar calibration can significantly deteriorate the performance of $\hat{\alpha}_H$. The algorithm based on Z_H (arbitrarily chosen) corrected attenuation to an accuracy of 30%. This accuracy was achieved after ensuring that there was no bias in the reflectivity-based algorithms. However, this is not possible in practical application. The algorithm to correct differential attenuation based on Z_H and $Z_{\rm DR}(\hat{\alpha}_D)$ can correct to an accuracy of 10% on the average. Similarly, the algorithm to correct differential attenuation based on $K_{\rm DP}$ ($\hat{\alpha}_D^*$) can correct to an accuracy of 40% on the average. Once again, in spite of the reduced accuracy of $\hat{\alpha}_D^*$, the algorithm has the advantage of being immune to absolute calibration errors. The above-mentioned accuracies were obtained theoretically, including the effects of measurement errors. Direct verification of the above results is nearly impossible and indirect procedures are used to verify the accuracy in the attenuation correction procedure.

Data collected by the C-band dual-polarized radar operated by DLR were utilized to verify the attenuation correction procedures. Theoretical evaluation indicated that the two attenuation correction procedures, namely, $\hat{\alpha}_H$ and $\hat{\alpha}_H^*$, should agree with each other in the mean. In addition the error structure of the intercomparison is a combination of the errors in $\hat{\alpha}_H$ and $\hat{\alpha}_H^*$. Theoretical analysis comparing $\hat{\alpha}_H$ versus $\hat{\alpha}_H^*$ shows that the accuracy of the intercomparison is approximately 20%–30%. Similarly theoretical analysis yielded that algorithms to correct for differential attenuation, namely, $\hat{\alpha}_D$ and $\hat{\alpha}_D^*$, can be compared to an accuracy of 30%–40%. Data from C-band dual-polarized radar were analyzed to intercompare the two attenuation correction algorithms $\hat{\alpha}_H$ and $\hat{\alpha}_H^*$. The two attenuation correction algorithms $\hat{\alpha}_H$ and $\hat{\alpha}_H^*$ agreed with each other fairly well and the FSE in the intercomparison was between 20% and 40% for specific attenuation higher than 0.1 dB km^{-1}, which is in excellent agreement with theoretical results presented in this paper. Similarly, the two algorithms to correct the differential attenuation, namely, $\hat{\alpha}_D$ and $\hat{\alpha}_D^*$, compared fairly well with each other. Thus the intercomparison study of the attenuation correction algorithms based on radar data provides an indirect verification of the theoretical results on the accuracies of the algorithms.

Acknowledgments. This research was supported partially by the Nationalb Group for Defense from Hydrological Hazard (CNR, Italy), by Progetto Strategico Mesoscale Alpine Programme (CNR, Italy), COST-75 (STSM), and by NASA (TRMM). The authors are grateful to P. Iacovelli for assistance rendered during the preparation of the manuscript.

REFERENCES

Aydin, K., Y. Zhao, and T. A. Seliga, 1989: Rain-induced attenuation effects on C-band dual-polarization meteorological radars. *IEEE Trans. Geosci. Remote Sens.*, **27,** 57–66.

Beard, K. V., and C. Chuang, 1987: A new model for the equilibrium shape of raindrops. *J. Atmos. Sci.*, **44,** 1509–1524.

Bringi, V. N., and A. Hendry, 1990: Technology of polarization diversity radars for meteorology. *Radar in Meteorology*, D. Atlas, Ed., Amer. Meteor. Soc., 153–190.

——, V. Chandrasekar, N. Balakrishnan, and D. S. Zrnić, 1990: An examination of propagation effects in rainfall on radar measurements at microwave frequencies. *J. Atmos. Oceanic Technol.,* **7,** 829–840.

Chandrasekar, V., V. N. Bringi, and P. J. Brockwell, 1986: Statistical properties of dual-polarized radar signals. Preprints, *23d Conf. on Radar Meteorology,* Snowmass, CO, Amer. Meteor. Soc., 193–196.

——, W. A. Cooper, and V. N. Bringi, 1988: Axis ratios and oscillations of raindrops. *J. Atmos. Sci.,* **45,** 1323–1333.

Gorgucci, E., G. Scarchilli, and V. Chandrasekar, 1995: Radar and raingage measurements of rainfall over the Arno basin. Preprints, *Conf. on Hydrology,* Dallas, TX, Amer. Meteor. Soc., 68–73.

Hildebrand, P. H., 1978: Iterative correction for attenuation of 5 cm radar in rain. *J. Appl. Meteor.,* **17,** 508–514.

Scarchilli, G., E. Gorgucci, V. Chandrasekar, and T. A. Seliga, 1993: Rainfall estimation using polarimetric techniques at C-band frequencies. *J. Appl. Meteor.,* **32,** 1150–1159.

Schroth, A., M. Chandra, and P. F. Meischner, 1988: A C-band coherent polarimetric radar for propagation and cloud physics research. *J. Atmos. Oceanic Technol.,* **5,** 803–822.

Seliga, T. A., and V. N. Bringi, 1976: Potential use of the radar reflectivity at orthogonal polarizations for measuring precipitation. *J. Appl. Meteor.,* **15,** 69–76.

Ulbrich, C. W., 1983: Natural variations in the analytical form of raindrop size distributions. *J. Climate Appl. Meteor.,* **22,** 1764–1775.